

# Neural Teleportation

Marco Armenta<sup>a,1,\*</sup>, Thierry Judge<sup>a,1</sup>, Nathan Painchaud<sup>a</sup>, Youssef Skandarani<sup>b</sup>, Carl Lemaire<sup>a</sup>, Gabriel Gibeau Sanchez<sup>a</sup>, Philippe Spino<sup>a</sup>, Pierre-Marc Jodoin<sup>a</sup>

<sup>a</sup>2500 Boulevard de l'Université, Sherbrooke, Quebec, Canada  
<sup>b</sup>Université Bourgogne, France

## Abstract

In this paper, we introduce *neural teleportation*, a simple operation one can use to initialize the weights of a neural network and gain faster convergence. Neural teleportation is the consequence of applying isomorphisms of quiver representations to neural networks. This process “*teleports*” a network to a new position in the weight space while leaving its input-to-output function unchanged. The concept of neural teleportation generalizes to any neural network architecture, activation function and task. We run several experiments that validate our hypothesis: teleporting a network at initialization speeds-up convergence. Finally, we discuss several mathematical and empirical findings concerning teleportation.

**Keywords:** quiver representations, neural networks, teleportation, network initialization.

**2010 MSC:** 68T01, 62M45, 16G20

## 1. Introduction

Despite years of research, our theoretical understanding of neural networks, their loss landscape and their behavior during training and testing is still limited. A recent novel theoretical analysis of neural networks using quiver representation theory [1] has been introduced, where the algebraic and combinatorial nature of neural networks is exposed. Among other things, the authors present a by-product of representing neural networks through the lens of quiver representation theory, *i.e.*, the notion of *neural teleportation*.

As will be explained later, neural teleportation is given by applying isomorphisms of quiver representations to neural networks. This process has the property of changing the weights and the activation functions of a network while, at the same time, preserving its function, *i.e.*, a teleported network makes the same predictions for the same input values as the original, non-teleported network.

Isomorphisms of quiver representations have already been used on neural networks, often unbeknownst to the authors, through the concept of *positive scale invariance* (also called *positive homogeneity*) of ReLU networks [2, 3, 4, 5]. This concept derives from the fact that one can choose a positive number  $c$  on each hidden neuron of a network (with ReLU, for example), multiply every incoming weight to that neuron by  $c$  and divide every outgoing weight by  $c$  and still have the same network function. In previous works [4, 6, 7, 8], positive homogeneity is restricted to positive scale invariant activation functions and to positive scaling factors, unlike for neural teleportation that works for any activation function. Models like maxout networks[9], leaky rectifiers[10] and deep linear networks[11] are also positive scale invariant.

In this paper, we show that neural teleportation has concrete consequences on the loss landscape and network optimization. Our findings can be summarized by the following 3 points:

1. Teleporting a network right after the usual initialization speeds-up convergence. We validate this for different datasets, activation functions, neural architectures and learning rates on gradient descent with and without momentum for supervised classification. We further underline this property with a theorem that expresses the gradient of a teleportation in terms of the original gradient and the chosen isomorphism;
2. Neural teleportation can be used to explore loss level curves;
3. *Micro-teleportation vectors* are rigorously perpendicular to back-propagated gradients computed with any kind and amount of labeled data, even random data with random labels;

\*Corresponding author

\*\*Our results can be reproduced with the code available here: [github.com/vitalab/neuralteleportation](https://github.com/vitalab/neuralteleportation).

Email addresses: marco.antonio.armenta@usherbrooke.ca (Marco Armenta), thierry.judge@usherbrooke.ca (Thierry Judge), nathan.painchaud@usherbrooke.ca (Nathan Painchaud), youssef\_skandarani@etu.u-bourgogne.fr (Youssef Skandarani), carl.lemaire@usherbrooke.ca (Carl Lemaire), gabriel.gibeau.sanchez@usherbrooke.ca (Gabriel Gibeau Sanchez), philippe.spino@usherbrooke.ca (Philippe Spino), pierre-marc.jodoin@usherbrooke.ca (Pierre-Marc Jodoin)

<sup>1</sup>Both authors contributed equally to this project.

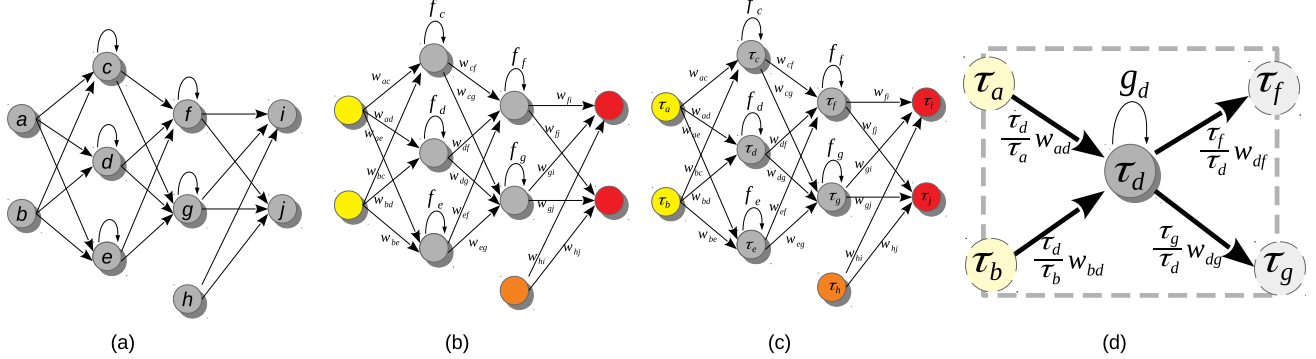


Figure 1: (a) Network quiver  $Q$  as introduced in [1]. (b) Neural network based on  $Q$  with weights  $W$  and activation functions  $f$ . Input, hidden, bias, and output neurons are in yellow, gray, orange and red, respectively. (c) Same neural network but with a change of basis (CoB)  $\tau_\epsilon$  at each neuron  $\epsilon$ . (d) Neural teleportation of the weights attached to neuron  $d$ . The resulting activation function is  $g_d(x) = \tau_d f_d(x/\tau_d)$ .

## 2. Neural teleportation

In this section, we explain what neural teleportation is. For more details on the theoretical interpretation of neural networks according to quiver representation theory, please refer to [1].

### 2.1. Isomorphisms and Change of Basis (CoB)

Neural networks are often pictured as oriented graphs. The authors in [1] show that neural network graphs are a specific kind of quiver with a loop at every node. They call these graphs *network quivers* (c.f. figure 1(a)). They also mention that neural networks, as they are generally defined, are network quivers with a weight assigned to every edge and an activation function at every loop (c.f. figure 1(b)).

According to representation theory, two quiver representations are equivalent if an *isomorphism* exists between the two. It was proved in [1], that isomorphisms of quiver representations can be formally extended to neural networks.

These isomorphisms are given by sets of non-zero real numbers assigned to the neurons of a neural network, subject to some conditions. One such set of non-zero numbers is called a *change of basis* (CoB) [12]. In order to apply an isomorphism to a neural network, each neuron must be assigned a CoB represented by  $\tau_\epsilon \in \mathbb{R}^{\neq 0}$  in figure 1(c).

The process of applying an isomorphism that respects the architecture of a neural net is called *neural teleportation*. For a teleportation to be valid, the CoB must comply to the following four conditions:

1. The CoB of every input, output and bias neuron must be equal to 1 (i.e.  $\tau_a, \tau_b, \tau_h, \tau_i, \tau_j = 1$  in figure 1(c)).
2. Neurons  $k, l$  connected by a residual connection should have the same CoB :  $\tau_k = \tau_l$ .
3. For convolutional layers, the neurons of a given feature map should share the same CoB.
4. For batch norm layers, an arbitrary non-zero CoB must be assigned to parameters  $\beta$  and  $\gamma$ , and for mean and variance the CoB should be equal to 1.
5. The CoBs of a dense connection are obtained by concatenating those in its input layers.

Condition 1 is the *isomorphism condition*. Any two networks related by a CoB satisfying this condition are said to be *isomorphic*. This leads to the following theorem proved in [1].

**Theorem 2.1.** *Isomorphic neural networks have the same network function.*

Said otherwise, despite having different weights and different activation functions, isomorphic neural networks return rigorously *the same predictions given the same inputs*. It also means that they have *exactly* the same loss value for any kind of input data, whenever the loss function doesn't depend directly on the weights. Nevertheless, even if they have different loss because of, for example,  $L_2$  regularization, the two networks will still have the same accuracy as they have the same network function. What changes is the behaviour of the training and the local loss landscape.

Conditions 2 to 5 have to do with the architecture of the network. They ensure that the produced isomorphic networks share the same architecture (c.f. [1] for more details). These conditions ensure that the teleportation of a residual connection remains a residual connection (condition 2), the teleportation of a conv layer remains a conv layer (condition 3), the teleportation of a batch norm layer remains a batch norm layer (condition 4) and the teleportation of a dense layer remains a dense layer (condition 5). Please note that Meng *et al.* [4] introduced condition 3 for ReLU networks, and that our condition 4 is not the same notion considered in [13].

## 2.2. Teleporting a neural network

Neural teleportation is a process by which the weights  $W$  and the activation functions  $f$  of a neural network are converted to a new set of weights  $V$ , and a new set of activation functions  $g$ . From a practical standpoint, neural teleportation is a simple process and is illustrated in figure 1(d).

Considering  $w_{ab} \in \mathbb{R}$  the weight of the connection from neuron  $a$  to neuron  $b$ , and  $\tau_a \in \mathbb{R}^{\neq 0}$  (resp.  $\tau_b \in \mathbb{R}^{\neq 0}$ ) the CoB of neuron  $a$  (resp.  $b$ ), the teleportation of that weight is simply:

$$v_{ab} = \frac{\tau_b}{\tau_a} w_{ab}. \quad (1)$$

To teleport an entire network, this operation is carried out for every weight of the network. Note that positive homogeneity [2, 3, 4, 5] is given by the same operation but with the restriction to positive CoB (that they call scaling factors). In the case of batch norm layers, the parameter  $\gamma$  is treated like a weight between two hidden neurons and  $\beta$  as a weight starting from a bias neuron. As such,  $\gamma$  and  $\beta$  are teleported just like any other weight using Eq.(1).

Neural teleportation is also applied to the activation functions. If  $f_d$  is the activation function of neuron  $d$  in figure 1(d), then the teleported activation function is

$$g_d(x) = \tau_d \cdot f_d \left( \frac{x}{\tau_d} \right). \quad (2)$$

This is a critical operation to make sure the pre- and post-teleported networks have the same network function. We can see that if  $\tau_d > 0$  and  $f_d$  is positive scale invariant (like ReLU) then  $g_d(x) = \tau_d f_d(x/\tau_d) = \tau_d / \tau_d f_d(x) = f_d(x)$ . Neural teleportation is thus a generalization of the concept of positive scale invariance [2, 3, 4, 5]. C.f. [1] for the formal proof.

## 3. Previous work

### 3.1. Initialization methods

By far the most common choices of weight initialization are given by randomly sampling a normal or uniform distribution with some variants like the Kaiming [10] and Xavier [14] methods. The LeCun method [15] initializes the weights of a network with activation functions that are differentiable at the origin, like tanh. Unfortunately, there is not a universally optimal initialization method. As pointed out by Hanin and Rolnick [16], an initialization method ill-suited to the architecture of a network can lead to training failures. In fact, looking for the right initialization method seems to be task dependant, and usually requires initialization search (and other hyperparameter search) to obtain optimal solutions [17].

But despite these corner cases, there has been limited research to improve the common *Kaiming* and *Xavier* methods. As noted by Goodfellow et al. [18]: “Modern initialization strategies are simple and heuristic. Designing improved initialization strategies is a difficult task because neural network optimization is not yet well understood”. In this paper, we propose a new initialization method that do not depend only on the sampling of a probability distribution function. We propose to apply the process of *neural teleportation* after the usual weight initialization. This means that teleportation is a second stage method. Said otherwise, once the weights are initialized, teleportation moves the weights to a place where the network function remains the same but the local normalized gradient has increased.

### 3.2. Positive scale invariance

It has been shown that positive scale invariance affects training by inducing symmetries on the weight space. As such, many methods have tried to take advantage of it [2, 5, 19, 20]. Our notion of teleportation gives a different perspective as (i) it allows any non-zero real-value CoB to be used as scaling parameters, (ii) it acts on any kind of activation functions, and (iii) our approach do not impose any constraints on the structure of the network nor the data it processes.

In [4, 5], the authors account for the fact that ReLU networks can be represented by the values of “basis paths” connecting input neurons to output neurons. Meng et al. [4] made clear that these paths are interdependent and proposed an optimization based on it. They designed a space that manages these dependencies, proposing an update rule for the values of the paths that are later converted back into network weights. Unfortunately, their method only works for neural nets having the same number of neurons in each hidden layer. Furthermore, they guarantee no invariance across residual connections. This is unlike neural teleportation, which works for any network architecture, including residual networks.

Scale-invariance in networks with batch normalization has been observed [13, 21], but not in the sense of quiver representations.

## 4. Theoretical analysis of teleportation

In this section, we outline our theoretical findings about teleportation to show some intuitions into its properties in relation to the gradient. In particular, we show that any teleportation increases the magnitude of the local normalized gradient.

#### 4.1. Back-propagated gradients of a teleportation

It has already been noticed [3, 5] that under positive scaling of ReLU networks, the weights scale proportionally to the CoB, and the gradient scales inversely with respect to the CoB. Here, we mathematically prove that the back-propagated gradient of a teleported network has the same property, regardless of the architecture of the network, the data and the activation functions.

Let  $(W, f)$  be a neural network with a set of weights  $W$  and activation functions  $f$ . Let also  $(V, g)$  be the weights and activation function of a network teleported from  $(W, f)$ . We denote  $W^{[\ell]}$  the weight matrix of the  $\ell$ -th layer of the network, and analogously for the teleportation  $V^{[\ell]}$ . The CoB  $\tau$  at layer  $\ell$  is denoted  $\tau^{[\ell]}$ , which is a column vector of non-zero real numbers. Following Eq. (1), we have that

$$V^{[\ell]} = \frac{1}{\tau^{[\ell-1]}} \bullet W^{[\ell]} \bullet \tau^{[\ell]}, \quad (3)$$

where the operation  $\frac{1}{\tau^{[\ell-1]}} \bullet W^{[\ell]}$  multiplies the columns of the matrix  $W^{[\ell]}$  by the coordinate values of vector  $\frac{1}{\tau^{[\ell-1]}}$ , while the operation  $W^{[\ell]} \bullet \tau^{[\ell]}$  multiplies the rows of matrix  $W^{[\ell]}$  by the coordinate values of the vector  $\tau^{[\ell]}$ .

Let's also consider a data sample  $(\mathbf{x}, t)$  with  $\mathbf{x}$  the input data and  $t$  the target value and  $dW, dV$  the gradients of the networks  $(W, f)$  and  $(V, g)$  with respect to  $(\mathbf{x}, t)$ . For the gradient, we have the following theorem.

**Theorem 4.1.** *Let  $(V, g)$  be a teleportation of the neural network  $(W, f)$  with respect to the CoB  $\tau$ . Then*

$$dV^{[\ell]} = \tau^{[\ell-1]} \bullet dW^{[\ell]} \bullet \frac{1}{\tau^{[\ell]}}$$

for every layer  $\ell$  of the network.

The proof of this theorem can be found in the appendix. From this result, it is easy to see that

$$\|dV\| = \sqrt{\sum_{i,j} \left( dW_{i,j} \frac{\tau_j}{\tau_i} \right)^2}. \quad (4)$$

Let  $0 \leq \sigma < 1$  be the CoB range to sample the CoB, that is, each CoB  $\tau_i$  is sampled from a uniform distribution on the interval  $[1 - \sigma, 1 + \sigma]$ . It is clear that  $\sigma = 0$  induces an identity transformation and therefore no teleportation. In the case where  $\sigma \rightarrow 1$  we have the following theorem.

**Theorem 4.2.** *When  $\sigma \rightarrow 1$ , the squared non-teleported gradient  $dW^2$  gets multiplied by an increasingly large factor.*

**Proof:** I We can see that the ratio  $\tau_a^2/\tau_b^2$  appears multiplying the squared non-teleported gradient  $dW^2$  in Eq. (4). Here, the CoBs  $\tau_i$  are sampled from a uniform distribution in an interval  $[1 - \sigma, 1 + \sigma]$  for  $0 \leq \sigma < 1$ . Observe that  $\sigma = 0$  implies that every  $\tau_i = 1$  and according to Eq. (3) and Eq. (2), the produced teleportation is the original network itself. Note also that for  $\sigma = 1$ , there exists the possibility of division by zero in Eq. (3).

Since  $\tau_a, \tau_b$  are independent random variables, the mathematical expectation of the squared ratio of both appearing in Eq. (4) is

$$\begin{aligned} \mathbb{E} \left[ \frac{\tau_a^2}{\tau_b^2} \right] &= \mathbb{E} \left[ \tau_a^2 \right] \cdot \mathbb{E} \left[ \frac{1}{\tau_b^2} \right] \\ &= \int_{1-\sigma}^{1+\sigma} \tau_a^2 P(\tau_a) d\tau_a \cdot \int_{1-\sigma}^{1+\sigma} P(\tau_b) / \tau_b^2 d\tau_b \\ &= \frac{\sigma^2 + 3}{3(1 - \sigma^2)}. \end{aligned}$$

Thus, when  $\sigma \rightarrow 0$  (i.e., no teleportation as mentioned above), then  $\mathbb{E} \left[ \frac{\tau_a^2}{\tau_b^2} \right] \rightarrow 1$  which means that on average the gradients are multiplied by 1 and thus remain unchanged. But when  $\sigma \rightarrow 1$ , then  $\mathbb{E} \left[ \frac{\tau_a^2}{\tau_b^2} \right] \rightarrow \infty$  which means that the gradient magnitude gets multiplied by an increasingly large factor. ■

These results suggest that teleportation when  $\sigma \rightarrow 1$  has a bigger impact in the local normalized gradient. Therefore, teleporting a network with a large  $\sigma$  boosts the gradient of the teleportation by an increasingly large value, and therefore it must accelerate training. We empirically validate this in section 5.

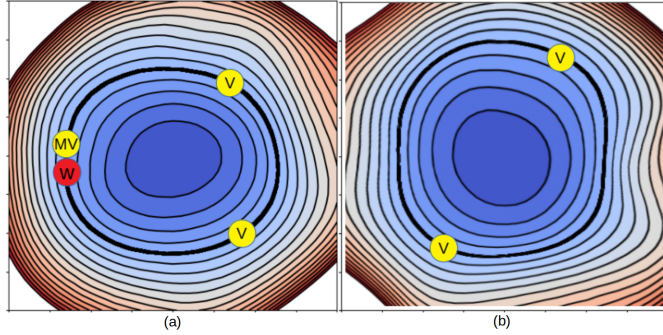


Figure 2: (a) 2D slice of a loss landscape with a  $W$  dot as the location of a given network. The  $V$  dots are two teleported versions of  $W$  inside the same landscape while the  $MV$  dot stands for a micro-teleportation of  $W$ . (b) The yellow dots are teleported versions of  $W$  in a different loss landscape. Since neural teleportation preserves the network function, the six networks have rigorously the same performance.

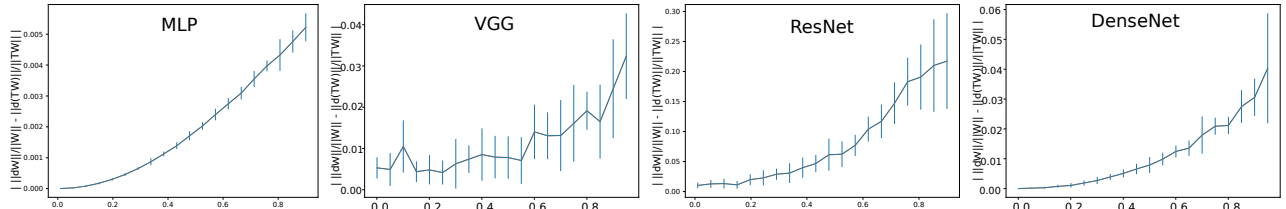


Figure 3: Mean absolute difference ( $\pm$  std-dev) between the back-propagated gradients' magnitudes of teleported networks and their original non-teleported network. Larger CoB generate larger gradients. Results are for CIFAR-10. Plots for these same models on CIFAR-100 can be found in the appendix.

#### 4.2. Empirical analysis of teleportation

The way the COB values  $\tau_i$  is chosen can greatly affect the teleportation process. For example, teleporting a positive scale invariant activation function  $f_d$  (like ReLU) with a positive  $\tau_d$  results in  $g_d = f_d$ . This means that the teleported network ends up inside the same loss landscape but with weights  $V$  at a different location than  $W$  (c.f., figure 2(a)). In other cases (for  $\tau_d$  negative or non-positive scale invariant activation functions  $f_d$ ) neural teleportation changes the activation function and thus the overall loss landscape. For example, with  $\tau_d < 0$  and  $f_d$  a ReLU function, the teleportation of  $f_d$  becomes:  $g_d(x) = \tau_d \max(0, x/\tau_d) = \min(0, \tau_d x/\tau_d) = \min(0, x)$ . Of course, a trivial case occurs when  $\tau_\epsilon = 1$  for every hidden neuron  $\epsilon$ , which leads to the identity transformation:  $V = W$  and  $g = f$ .

As such, we explore two different ways of computing the COB values. The first one is by randomly sampling a uniform distribution centered on 1:  $\tau_\epsilon \in [1 - \sigma, 1 + \sigma]$  with  $0 \leq \sigma < 1$ . We call  $\sigma$  the *CoB-range*; the larger  $\sigma$  is, the more different the teleported network weights  $V$  will be from  $W$ . Also, when this sampling operation is combined with positive scale invariant activation function (like ReLU), the teleported activation functions remains unchanged ( $g = f$ ) and thus the new weights  $V$  are guaranteed to stay within the same landscape as the original set of weights  $W$  (as in figure 2 (a)). We thus call this operation an *intra-landscape* neural teleportation.

The other distribution is a mixture of two equal-sized uniform distributions: one centered at +1 and the other at -1, that is,  $\tau_\epsilon \in [1 - \sigma, 1 + \sigma] \cup [-1 - \sigma, -1 + \sigma]$ . With high probability, a network teleported with this sampling will end up in a new loss landscape as illustrated in figure 2 (b). We thus call this operation an *inter-landscape* neural teleportation. This is the type of teleportation we use for all our training experiments in Section 5.

We empirically validate the hypothesis that teleportation has the effect of boosting gradients with four different networks and two datasets (CIFAR10 and CIFAR100). In each case, we teleported the network with different  $\sigma$  values and computed the mean absolute difference between the back-propagated gradients of the original network ( $W, f$ ) and the teleported network ( $V, g$ ).

Results are reported in figure 3 where the CoB-range  $\sigma$  is on the x-axis and the y-axis is the absolute difference of normalized gradient magnitude:

$$\|dW\|/\|W\| - \|dV\|/\|V\|.$$

Results reveal that, as shown by our theoretical analysis, a larger CoB-range leads to a larger normalized gradient magnitude. Said otherwise, randomly teleporting a neural network with a large  $\sigma$  value increases how steep is the surrounding landscape

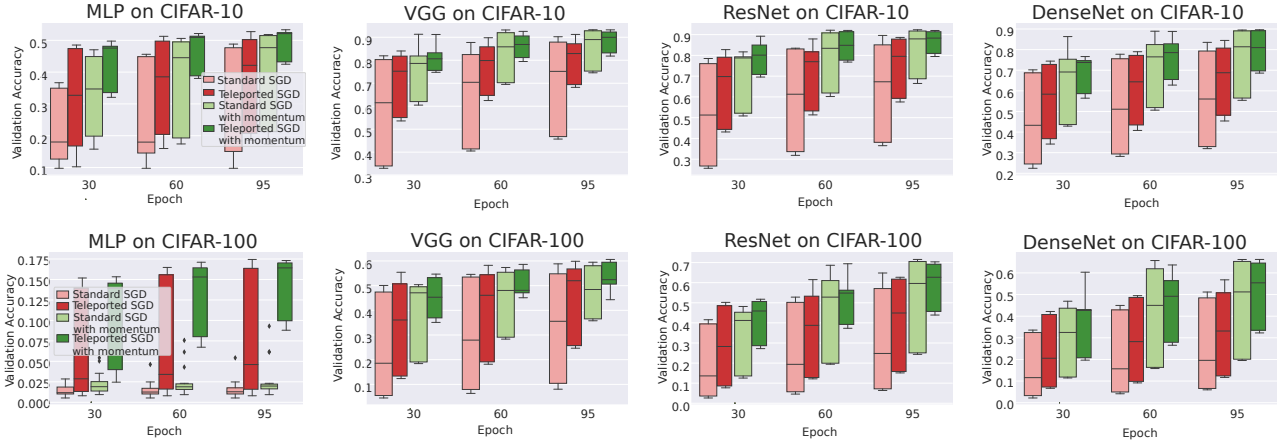


Figure 4: Validation accuracies for MLP, VGG, ResNet and DenseNet on CIFAR-10 (top row) and CIFAR-100 (bottom row). The boxes are produced with 5 runs for every learning rate (0.01, 0.001 and 0.0001). Note that the MLP on CIFAR-100 does not seem to move towards convergence without teleportation.

and also increases the magnitude of the local normalized gradient. This works for any network architecture and any dataset. This analysis also holds true for *inter*-landscape CoB sampling since the CoB terms appear squared in Eq. (4).

## 5. Convergence speed up

An immediate consequence of the previous section is that teleporting a network just after its initialization sets it in an area of the landscape where the slope is steeper and the normalized gradient has a higher magnitude, which can produce a faster change on the weights during training, and even accelerate it.

In order to assess this statement, we trained four models: an MLP with 5 hidden layers with 500 neurons each, a VGGnet with batch normalization layers, a ResNet18, and a DenseNet, all with ReLU activation. Training was done on two datasets (CIFAR-10 and CIFAR-100) with two optimizers (vanilla SGD and SGD with momentum), and three different learning rates (0.01, 0.001 and 0.0001) for a total of 72 configurations. For each configuration, we trained the network with and without neural teleportation after initialization. Training was done five times for 100 epochs. The chosen CoB range  $\sigma$  is 0.9 with an *inter*-landscape sampling for all these experiments (so ReLU changes for  $g(x) = \min(0, x)$  roughly 50% of the times). The teleported and non-teleported networks were initialized with the same randomized operator following the “Kaiming” method.

This resulted into a total of 720 training curves that we averaged across the learning rates. The resulting box plots are shown in figure 4. The light green and light red boxes are results from usual training while the dark green and dark red boxes are results from the same training settings but applying neural teleportation (to each network) after initialization. As can be seen, neural teleportation accelerates the convergence of every model, on every dataset and every optimizer. Note that we show validation accuracy in our plots.

To make sure that these results are not unique to ReLU networks, we trained the MLP on MNIST and CIFAR-10 with three different activation functions : LeakyReLU, Tanh and ELU, again with and without neural teleportation after the uniform initialization, which is the default PyTorch init mode for fully connected layers. As can be seen from figure 5, here again teleportation accelerates training across datasets and models.

In order to measure the impact of the initialization procedure, we ran a similar experiment with a basic Gaussian initialization as well as an Xavier initialization. We obtained the same pattern for the former and the latter: teleportation helps the training of the VGG net, while for the others the difference is less prominent (see figure 6). Note, however, that teleportation doesn't disrupt the training result.

Figure 7(left) shows the weight histograms of an MLP network initialized with a uniform distribution (PyTorch's default) before and after teleportation. As can be seen, the weight distributions are significantly different. Teleportation ends up pushing several weights towards the origin while, at the same time, pushing others away from the origin leading to an heavy-tail distribution. In order to assess whether the training benefits observed thus far was attributed to the second distribution, we initialized the weights of four neural networks by randomly sampling the distribution of Figure 7(right). We called this a *pseudo-teleportation*. We then trained the models with the same regime, comparing pseudo-teleportation to no teleportation. Results in figure 8 reveal that pseudo-teleportation does not improve training systematically like teleportation does.

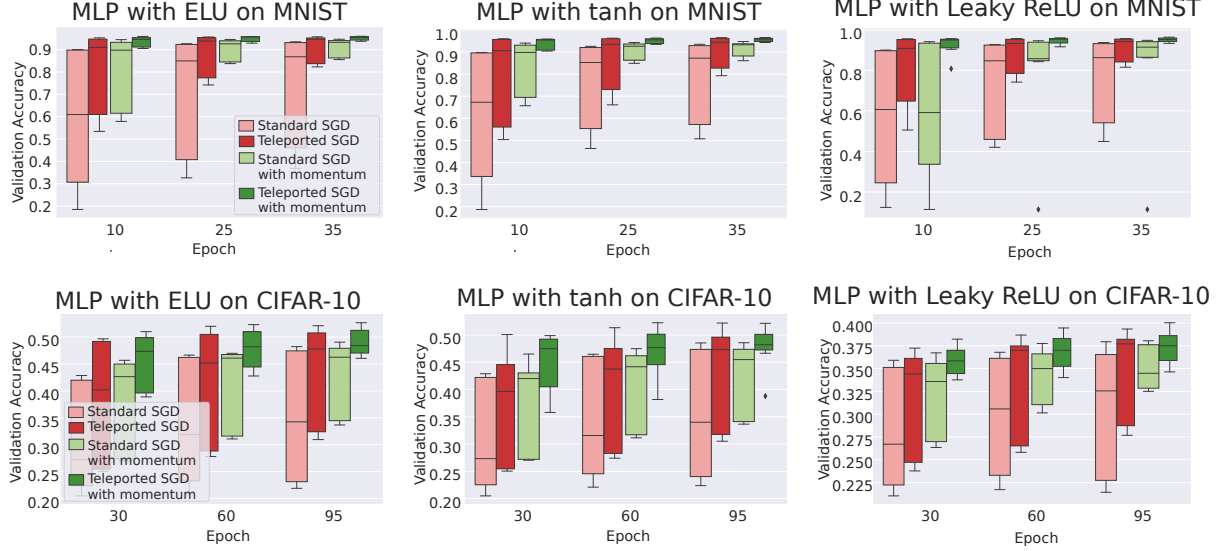


Figure 5: Validation plots produced over 5 runs over three learning rates (0.01, 0.001 and 0.0001) of MLPs with activations LeakyReLU (first column), Tanh (second column) and ELU (third column) resp., on MNIST (top row) and CIFAR-10 (bottom row) datasets.

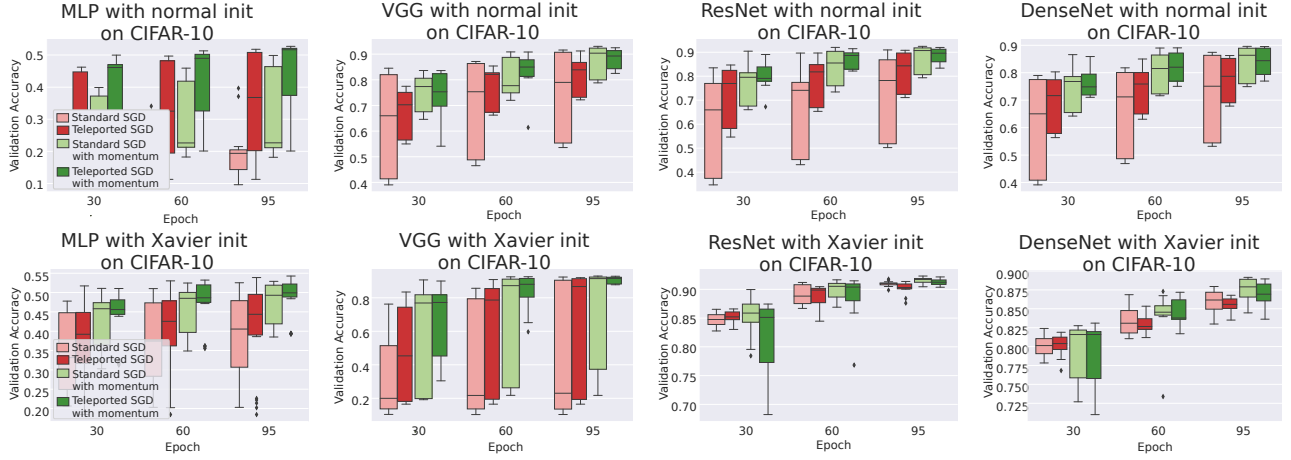


Figure 6: Validation plots produced over 5 runs over three learning rates (0.01, 0.001 and 0.0001) for MLP, VGG, ResNet and DenseNet with normal (top row) and Xavier (bottom row) initializations on CIFAR-10.

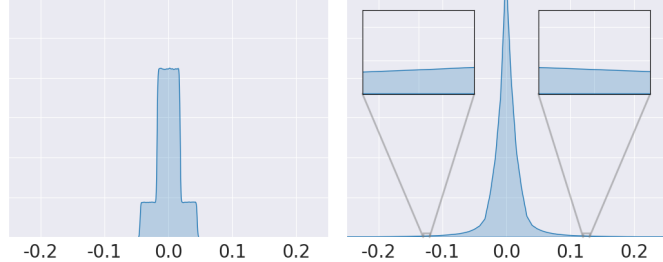


Figure 7: Weight histogram of an MLP before teleportation [Left] and after teleportation [Right] with CoB-range of 0.9. Initialization is the standard on PyTorch which is uniform and contains values between  $-0.05$  and  $0.05$  while the teleported weights are more broadly distributed as shown in the zooms.

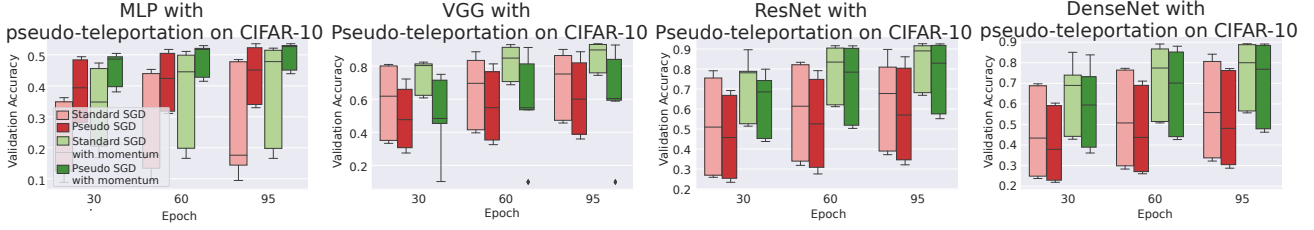


Figure 8: Validation plots produced over 5 runs over three learning rates (0.01, 0.001 and 0.0001) for MLP, VGG, ResNet and DenseNet on CIFAR-10 comparing a usual training and a training with pseudo-teleportation. It can be seen that pseudo-teleportation helps the training of the MLP, but it worsens the training for the other models.

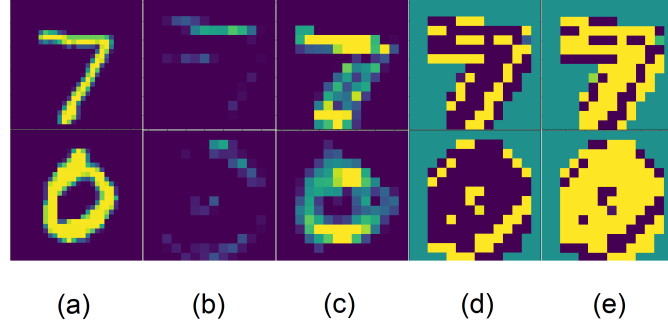


Figure 9: (a) MNIST images. (b) Feature maps of a trained ReLU ResNet18. (c) Same feature maps after teleportation. (d) Feature maps of a trained tanh ResNet18. (e) Same feature maps after teleportation.

## 6. Discussion

In this final section, we discuss some theoretical and empirical findings about neural teleportation.

### 6.1. Feature maps

In order to put forward more concretely the effect that neural teleportation has on a neural network, we trained (on MNIST) and teleported (after training) two ResNet18 models: one with ReLU activations and one with tanh activations. Feature maps of the original and teleported trained networks are shown in figure (9). As one can see, the feature maps before and after teleportation are, in both cases, very different. This underlines the fact that while teleportation preserves the network function (and thus doesn't change the performance of the network) it drastically changes the features that the network has learned.

### 6.2. Loss level curves

Since each CoB  $\tau_\epsilon$  can be assigned any non-zero real values, a network can be teleported an infinite amount of times to an infinite amount of locations within the same landscape or across different landscapes. This is illustrated in figure 2 where  $W$  is teleported to 5 different locations in two different loss landscapes. Because of the nature of neural teleportation, which preserves the network function, these 6 neural networks have the same loss value (whenever the loss doesn't include a regularization term that involves the weights). Thus, teleported networks *sit on the same loss level curve*.

We validated this assertion by teleporting an MLP 100 times with an inter-landscape sampling and a CoB-range of  $\sigma = 0.9$ . While the mean average difference between the original weights  $W$  and the teleported weights  $V$  is of 0.08 (a large value considering that the magnitude of  $W$  is of 0.18), the average loss difference was of  $10^{-10}$ , *i.e.*, no more than a floating point error.

### 6.3. Micro teleportation

One can prove that the gradient of a function is always perpendicular to its local level curve (c.f. [22] chap. 2). But in principle, one wouldn't expect this to hold even on random data with random labels across different architectures with different batch-sizes, because the cost is computed as an average over the batch of data.

This concern can be explored via the notion of *micro-teleportation*, which derives from the previous subsection. Let's consider the intra-landscape teleportation of a network with positive scale invariant activation functions (like ReLU) with a CoB-range  $\sigma$  close to zero. In that case,  $\tau_\epsilon \approx 1$  for every neuron  $\epsilon$  and the teleported weights  $V$  (computed following Eq.(1))

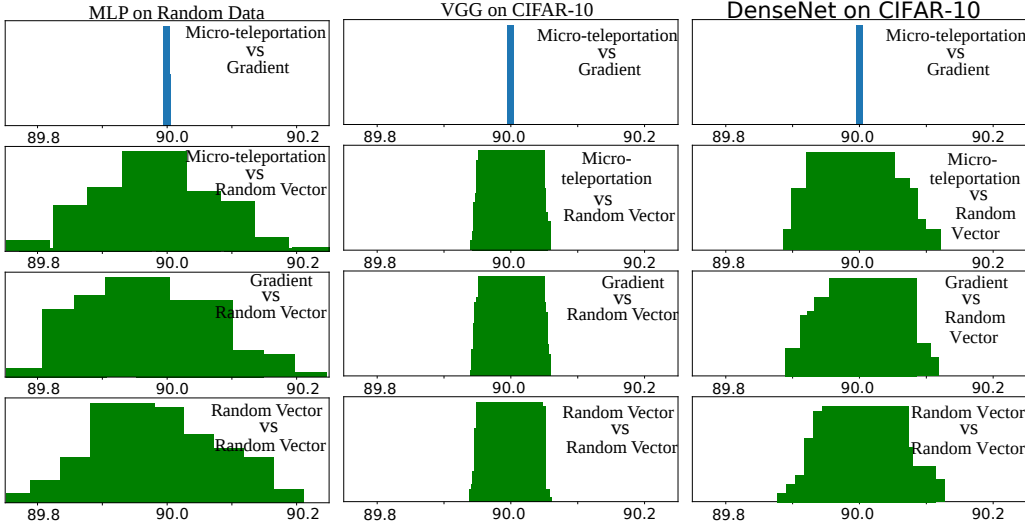


Figure 10: [Top] Angle histograms between micro-teleportation vectors and back-propagated gradients for VGGnet on CIFAR10 data and MLP on random data. The other rows are angle histograms between micro-teleportation vectors and random vectors, between gradient and random vectors and between random vectors.

end up being very close to  $W$ . We call this a *micro-teleportation* and illustrate it in figure (1) (a) (the MV dot illustrates the micro teleportation of  $W$ ).

Because  $V$  and  $W$  are isomorphic, they both lie on the same loss level curve. Thus, if  $\sigma$  is small enough, the vector  $\overrightarrow{WV}$  between  $W$  and  $V$  is locally co-linear to the local loss level curve. We call  $\overrightarrow{WV}$  a *micro-teleportation vector*.

A property of micro-teleportations is that the micro-teleportation vector  $\overrightarrow{WV}$  is perpendicular to any back-propagated gradient computed with any batch size and any kind of data, even random data with random labels. This observation leads to the following corollary.

**Corollary 6.1.** *For any neural network, any dataset and any loss function, there exists a sufficiently small CoB-range  $\sigma$  such that every micro-teleportation produced with it is perpendicular to the back-propagated gradient.*

Note that this statement is true for loss functions without a regularization term that depends on the weights, as L2 regularization. This is because regularization terms make the loss landscape dependent on weights that are affected by teleportation. However, even in the case of using L2 regularization, teleportation will produce a network with the same accuracy on the given data set even if the loss changes. We empirically assessed this by computing the angle between micro-teleportation vectors and back-propagated gradients of four models (MLP, VGG, ResNet and DenseNet) on three datasets (CIFAR-10, CIFAR-100 and random data) 2 different batch sizes (8 and 64) with a CoB-range  $\sigma = 0.001$ . A cross-entropy loss without regularization term was used for all models. Figure 10 shows angular histograms for VGG on CIFAR-10, an MLP (with one hidden layer of 128 neurons) on random data and DenseNet on CIFAR-10 (results for the other configurations can be found in the appendix). The first row shows the angular histogram between micro-teleportation vectors and back-propagated gradients. We used batch sizes of 8 for the MLP and DenseNet and 64 for VGG. As can be seen, the three histograms exhibit a clear Dirac delta on the  $90^\circ$  angle. As a mean of comparison, we report angular histograms between micro-teleportation vectors and random vectors, between back-propagated gradients and random vectors, and between random vectors. Note that random vectors in high dimensional spaces are known to be quasi-orthogonal [23]. In figure 10, the Dirac delta of the first row versus the wider green distributions is a clear illustration that the micro-teleportation vector is perpendicular to any back-propagated gradient.

#### 6.4. Teleportation and landscape flatness

Dinh *et al.* [3] showed that for positive scale invariant activation functions (like ReLU), one can find a CoB (called *reparametrization* in [3]) so that the most commonly used measures for flatness can be manipulated to obtain a sharper minimum with the exact same network function. We empirically show that neural teleportation systematically sharpens the found minima, independently of the architecture and the activation functions.

A commonly used method to compare the flatness of two trained networks is to plot the 1D loss/accuracy curves on the interpolation between the two sets of weights [3]. It is also well known that small batch sizes produce flatter minima than bigger batch sizes. We trained on CIFAR10 a 5 hidden-layer MLP two times, first with a batch size of 8 (network  $A$ ) then with

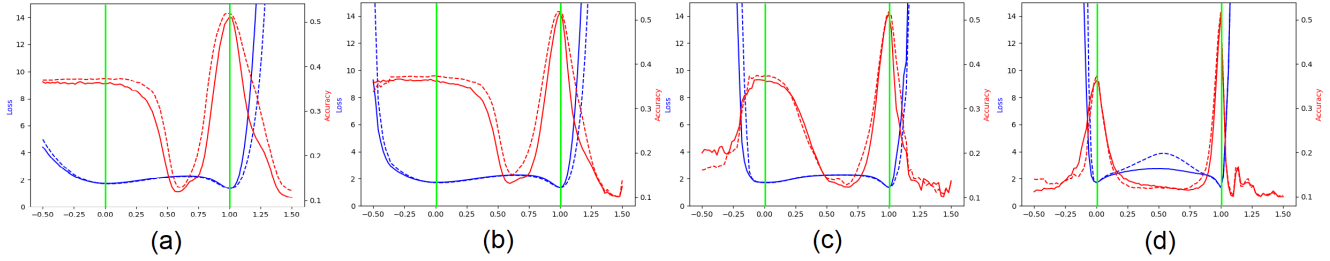


Figure 11: (a) Loss/accuracy profiles obtained by linearly interpolating between two optimized MLP  $A$  and  $B$ . Network  $A$  is for  $x = 0$  and  $B$  for  $x = 1$  (green vertical lines). Dotted lines are for training and solid lines for validation. Remaining plots are similar interpolations but between teleported versions of  $A$  and  $B$  with CoB range  $\sigma$  of (b) 0.6, (c) 0.9, and (d) 0.99.

a batch size of 1024 (network  $B$ ). Then, as in [24], we plotted the 1D loss/accuracy curves on the interpolation between the two weight vectors of the networks (c.f. figure 11(a)). We then performed the same interpolation but between the teleportations of  $A$  and  $B$  with CoB-ranges  $\sigma$  of 0.6, 0.9, and 0.99. As can be seen from figure 11, the landscape becomes sharper as the CoB-range increases. Said otherwise, a larger teleportation leads to a locally-sharper landscape. More experiments with other models can be found in the appendix.

## 7. Conclusion

Weight initialization is known to be a hard problem due to the lack of understanding of the training process of neural networks. We have developed a theoretical framework that suggests that the use of teleportation as a second-stage initialization produces a boost on the gradient.

Through extensive experimentation we have shown that applying neural teleportation right after the usual initialization methods produces faster convergence across different architectures and datasets. Teleportation is thus a second-stage initialization method that outperforms any other type of one-stage initialization by a big margin.

Here, we presented experimental results on supervised classification tasks, but all of our theoretical results hold true for any neural network independently of the task, for example, theorem 4.1 gives the structure of the gradient of any teleported network. In other words, the teleportation process can be applied to any neural network and it will have the same effect on the normalized gradient. We therefore have presented an initialization method that boosts the gradient and not only tries to break the symmetries in weight space as other initialization methods. Even more, we have demonstrated that teleportation with a large CoB range sharpens the local loss landscape, therefore giving a geometrical interpretation of the acceleration of convergence presented in our experiments.

## References

- [1] M. A. Armenta, P.-M. Jodoin, The representation theory of neural networks, arXiv:2007.12213, 2020.
- [2] V. Badrinarayanan, B. Mishra, R. Cipolla, Understanding Symmetries in Deep Networks, arXiv:1511.01029, 2015.
- [3] L. Dinh, R. Pascanu, S. Bengio, Y. Bengio, Sharp Minima Can Generalize for Deep Nets, in: proc. of ICML, Vol. 70 of Proceedings of Machine Learning Research, PMLR, 2017, p. 1019–1028.
- [4] Q. Meng, S. Zheng, H. Zhang, W. Chen, Q. Ye, Z. Ma, N. Yu, T. Liu, G-SGD: Optimizing ReLU Neural Networks in its Positively Scale-Invariant Space, in: proc. of ICLR, 2019.
- [5] B. Neyshabur, R. Salakhutdinov, N. Srebro, Path-SGD: Path-Normalized Optimization in Deep Neural Networks, in: proc. of NIPS, MIT Press, 2015, p. 2422–2430.
- [6] L. Meng, J. Zhang, IsoNN: Isomorphic Neural Network for Graph Representation Learning and Classification, arXiv:1907.09495, 2019.
- [7] M. Yi, Q. Meng, W. Chen, Z. Ma, T. Liu, Positively Scale-Invariant Flatness of ReLU Neural Networks, arXiv:1903.02237, 2019.
- [8] J. Zhu, Q. Meng, W. Chen, Z. Ma, Interpreting the basis path set in neural networks, Journal of Systems Science and Complexity, 2021, p. 1559–7067.

- [9] I. J. Goodfellow, D. Warde-Farley, C. Mirza, Mehdi, A. C., Y. Bengio, Maxout networks, in: proc. of ICML, Vol. 3, 2013, p. 1319–1327.
- [10] K. He, X. Zhang, S. Ren, J. Sun, Delving deep into rectifiers: Surpassing human-level performance on imagenet classification, in: 2015 IEEE ICCV, 2015, pp. 1026–1034.
- [11] A. M. Saxe, J. L. McClelland, S. Ganguli, Exact solutions to the nonlinear dynamics of learning in deep linear neural network, in: proc. ICLR, 2014.
- [12] I. Assem, D. Simson, A. Skowronski, Elements of the Representation Theory of Associative Algebras. Vol. 1: Techniques of Representation Theory, Vol. 65 of London Mathematical Society Student Texts, Cambridge Univ. Press., Cambridge, 2006.
- [13] S. Arora, Z. Li, K. Lyu, Theoretical analysis of auto rate-tuning by batch normalization, in: proc. of ICLR, 2019.
- [14] X. Glorot, Y. Bengio, Understanding the difficulty of training deep feedforward neural networks, in: proc. of MLR, Vol. 9, 2010, pp. 249–256.
- [15] LeCun Y.A. and Bottou L. and Orr G.B. and Müller KR., Efficient backprop, Neural Networks: Tricks of the Trade. Lecture Notes in Computer Science 7700, 2012.
- [16] B. Hanin, D. Rolnick, How to start training: The effect of initialization and architecture, in: proc. NIPS, Vol. 31, Curran Associates, Inc., 2018.
- [17] C.-K. Dowa, Afiahayati, Suitable cnn weight initialization and activation function for javanese vowels classification, Procedia Computer Science 144, p. 124–132, 2018.
- [18] I. Goodfellow, Y. Bengio, A. Courville, Deep Learning, MIT Press, 2016.
- [19] V. Badrinarayanan, B. Mishra, R. Cipolla, Symmetry-invariant optimization in deep networks, arXiv:1511.01754, 2015.
- [20] L. Huang, X. Liu, J. Qin, F. Zhu, L. Liu, L. Shao, Projection based weight normalization: Efficient method for optimization on oblique manifold in dnns, Pattern Recognition 105, 2020.
- [21] M. Cho, J. Lee, Riemannian approach to batch normalization, in: proc. of NIPS, Curran Associates Inc., 2017, p. 5231–5241.
- [22] M. Spivak, Calculus on Manifolds: A Modern Approach to Classical Theorems of Advanced Calculus, Mathematics Monograph Series, Addison-Wesley Publishing Company, 1965.
- [23] P. C. Kainen, V. Kůrková, Quasiorthogonal Dimension, Springer International Publishing, 2020, pp. 615–629.
- [24] H. Li, Z. Xu, G. Taylor, C. Studer, T. Goldstein, Visualizing the Loss Landscape of Neural Nets, in: proc. of NIPS, Curran Associates Inc., 2018, p. 6391–6401.

## Appendix

### Convergence speed up

Following section 5, we present in figure 15 the validation accuracy box plots obtained with normal and Xavier initializations on the CIFAR-100 dataset. We also show in figure 16 some more pseudo-teleportation results for MLP, VGG, ResNet and DenseNet on CIFAR-100.

### Micro-teleportations

Following section 4.3 on micro-teleportations, we provide more angular histograms between back-propagated gradients and random micro-teleportations of the network. We present here some more histograms for models MLP, VGG, ResNet and DenseNet on datasets CIFAR-10, CIFAR-100 and random data. Each histogram in figure 12 was computed with 100 random micro-teleportations with a CoB-range  $\sigma = 0.001$ .

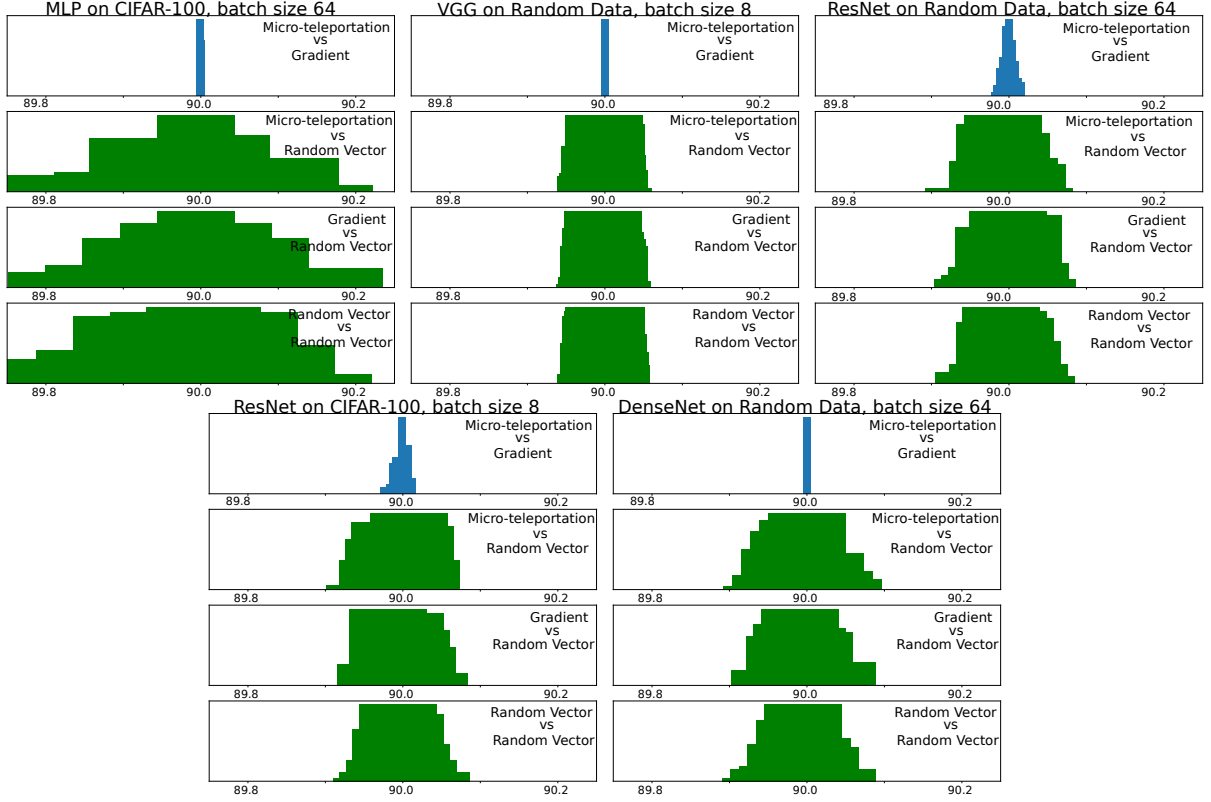


Figure 12: Micro teleportations

### Teleportation and landscape flatness

Following section 4.4, we trained a VGGnet with two different batch sizes and then produced a 1D loss plot by interpolating the two models. We then re-produced 1D loss plots by teleporting the models. As shown in figure 13, neural teleportation has the effect of sharpening the loss landscape.

### Back-propagated gradients of a teleportation

Here we give the proof of Theorem 4.1 and reproduce the experiment shown in figure 7 for the CIFAR-100 dataset. Results are shown in figure 14.

### Proof of Theorem 4.1

We will introduce the notation for a forward pass on a neural network  $(W, f)$  with  $L$  hidden layers without bias vertices for clarity. For the forward pass of  $(W, f)$  we first fix a data sample  $(x, t)$  and define the vector of activation outputs of neurons at layer  $\ell$  by  $a_W^{[\ell]}$ , and the vector of pre-activations at layer  $\ell$  by  $z_W^{[\ell]}$ . We will denote by  $f^{[\ell]}$  the vector of activation functions at layer  $\ell$ . For the input layer we have  $a_W^{[0]} = z_W^{[0]} = x$ . Next, we define inductively

$$z_W^{[\ell]} = W^{[\ell]} a_W^{[\ell-1]} \text{ and } a_W^{[\ell]} = f^{[\ell]}(z_W^{[\ell]}) \quad (5)$$

for every  $\ell = 1, \dots, L + 1$ .

In the case of the backward pass, we denote the vector of derivatives of activations in layer  $\ell$  by  $df^{[\ell]}$ , and the vector of derivatives with respect to the activation outputs of neurons on layer  $\ell$  by  $da_W^{[\ell]}$ . On the output layer we have

$$da_W^{[L+1]} = \frac{\partial \mathcal{L}}{\partial a_W^{[L+1]}}(a_W^{[L+1]}, y) \quad (6)$$

where  $\mathcal{L}$  is the loss function. If we denote by  $\odot$  the point-wise (Hadamard) product of vectors of the same size, then inductively from layer  $L + 1$  down to the input layer we have

$$dW^{[\ell]} = (da_W^{[\ell]} \odot df^{[\ell]}(z_W^{[\ell]})) a_W^{[\ell-1]^T}, \quad (7)$$

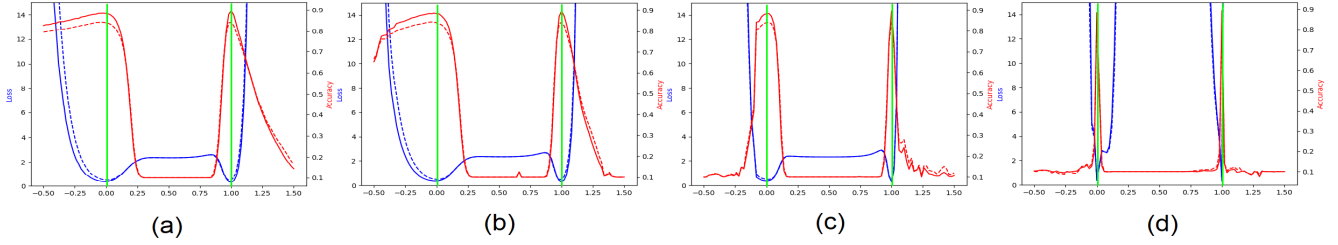


Figure 13: (a) Loss/accuracy profiles obtained by linearly interpolating between two optimized VGG  $A$  and  $B$ . Network  $A$  is for  $x = 0$  and  $B$  for  $x = 1$  (green vertical lines). Dotted lines are for training and solid lines for validation. Remaining plots are similar interpolations but between teleported versions of  $A$  and  $B$  with CoB range  $\sigma$  of (b) 0.6, (c) 0.9, and (d) 0.99.

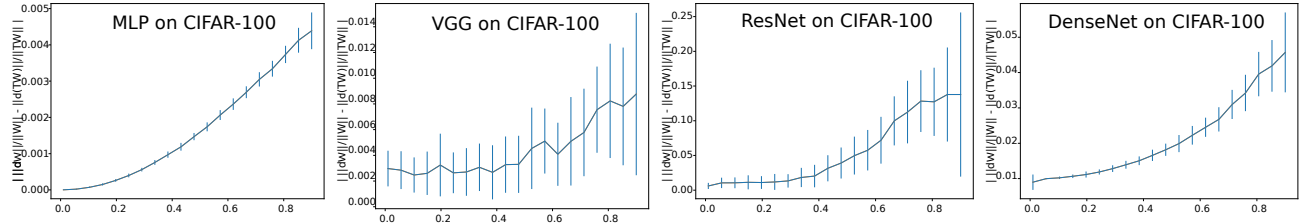


Figure 14: Mean absolute difference ( $\pm$  std-dev) between the back-propagated gradients' magnitudes of teleported networks and their original, not teleported, network. Larger CoB generate larger gradients.

and also that

$$da_W^{[\ell-1]} = \left( W^{[\ell]} \right)^T \left( da_W^{[\ell]} \odot df^{[\ell]} \left( z_W^{[\ell]} \right) \right). \quad (8)$$

If  $\tau : (W, f) \rightarrow (V, g)$  is an isomorphism of neural networks, given by a choice of change of basis in every hidden neuron and we denote by  $\tau^{[\ell]}$  the vector of change of basis for layer  $\ell$ , then

$$V^{[\ell]} = \frac{1}{\tau^{[\ell-1]}} \bullet W^{[\ell]} \bullet \tau^{[\ell]}. \quad (9)$$

and for the activation functions we have

$$g^{[\ell]}(x) = f^{[\ell]} \left( x \bullet \frac{1}{\tau^{[\ell]}} \right) \bullet \tau^{[\ell]}, \quad (10)$$

Where the operation  $\frac{1}{\tau^{[\ell-1]}} \bullet -$  on the left of a matrix, multiplies its columns by the coordinate values of vector  $\frac{1}{\tau^{[\ell-1]}}$ . While the operation  $- \bullet \tau^{[\ell]}$  on the right of a matrix, multiplies its rows by the coordinate values of the vector  $\tau^{[\ell]}$ . By transposing Eq. 9, we obtain

$$\left( V^{[\ell]} \right)^T = \tau^{[\ell]} \bullet \left( W^{[\ell]} \right)^T \bullet \frac{1}{\tau^{[\ell-1]}}. \quad (11)$$

By the chain rule and Eq. 10 we can see that

$$dg^{[\ell]}(x) = df^{[\ell]} \left( x \bullet \frac{1}{\tau^{[\ell]}} \right). \quad (12)$$

Also, from the proof of Theorem in 4.9 [1],

$$z_V^{[\ell]} = z_W^{[\ell]} \bullet \tau^{[\ell]} \quad \text{and} \quad a_V^{[\ell]} = a_W^{[\ell]} \bullet \tau^{[\ell]}. \quad (13)$$

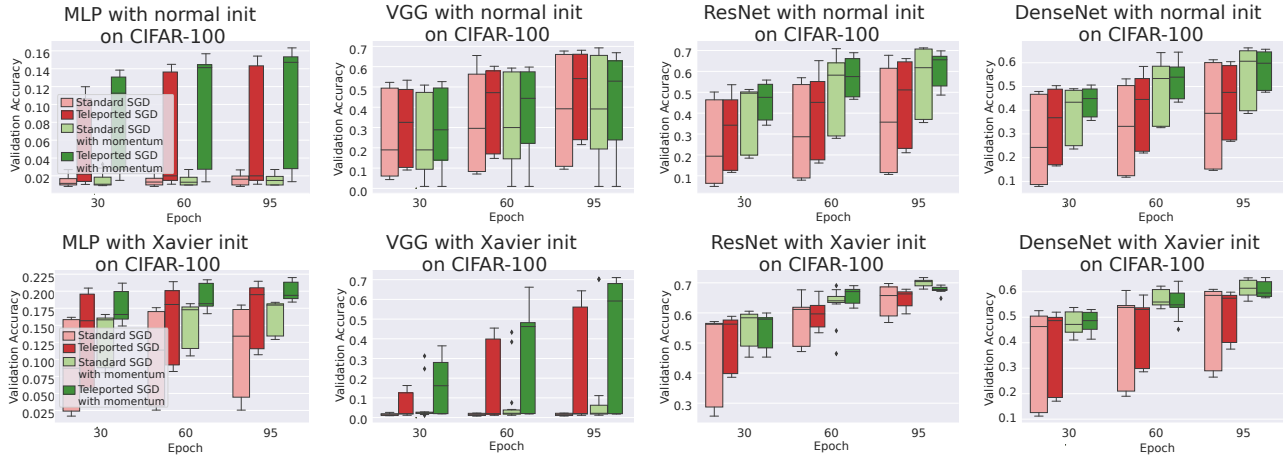


Figure 15: Validation plots produced over 5 runs over three learning rates (0.01, 0.001 and 0.0001) of the four models MLP, VGG, ResNet and DenseNet with normal (top row) and Xavier (bottom row) initializations on CIFAR-100.

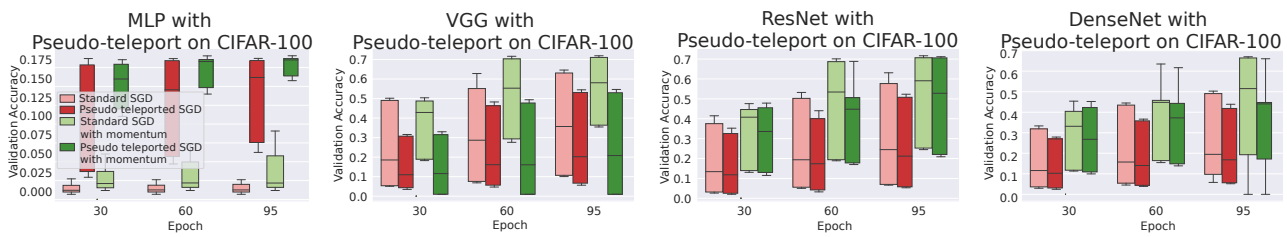


Figure 16: Validation plots produced over 5 runs over three learning rates (0.01, 0.001 and 0.0001) of the four models MLP, VGG, ResNet and DenseNet with pseudo-teleportation on CIFAR-100.

**Theorem 7.1.** Let  $(V, g)$  be a teleportation of the neural network  $(W, f)$  with respect to the CoB  $\tau$ . Then

$$dV^{[\ell]} = \tau^{[\ell-1]} \bullet dW^{[\ell]} \bullet \frac{1}{\tau^{[\ell]}}$$

for every layer  $\ell$  of the network.

**Proof:** We proceed by induction on the steps of the backward pass of the network  $(V, g)$ . By Theorem 4.9 of [1], both networks  $(W, f)$  and  $(V, g)$  give the same output  $a_W^{[L+1]} = a_V^{[L+1]}$ , so by Eq. 6 we get that  $da_W^{[L+1]} = da_V^{[L+1]}$ . We can substitute this together with Eq. 13 into Eq. 7 applied to the neural network  $(V, g)$  to obtain

$$\begin{aligned} dV^{[L+1]} &= da_V^{[L+1]} a_V^{[L]}^T \\ &= da_W^{[L+1]} \left( a_W^{[L]} \bullet \tau^{[L]} \right)^T \\ &= dW^{[L+1]} \bullet \frac{1}{\tau^{[L]}}. \end{aligned}$$

Now, the derivative of the loss function with respect to the activation outputs of layer  $L$  in  $(V, g)$  can be written analogously to Eq. 8, in which we substitute Eq. 11 taking into account that the CoB for the output layer is given by 1's, so we get

$$\begin{aligned} da_V^{[L]} &= (V^{[L+1]})^T da_V^{[L+1]} \\ &= (W^{[L+1]})^T \bullet \frac{1}{\tau^{[L]}} da_W^{[L+1]} \\ &= da_W^{[L]} \bullet \frac{1}{\tau^{[L]}}. \end{aligned}$$

At layer  $L$  we get that

$$\begin{aligned} dV^{[L]} &= \left( da_V^{[L]} \odot dg^{[L]} \left( z_V^{[L]} \right) \right) a_V^{[L-1]}^T \\ &= \left( da_W^{[L]} \bullet \frac{1}{\tau^{[L]}} \right) \odot df^{[L]} \left( z_W^{[L]} \bullet \tau^{[L]} \bullet \frac{1}{\tau^{[L]}} \right) a_V^{[L-1]}^T \\ &= \left( da_W^{[L]} \odot df^{[L]} \left( z_W^{[L]} \right) \bullet \frac{1}{\tau^{[L]}} \right) \left( a_W^{[L-1]} \bullet \tau^{[L-1]} \right)^T \\ &= \left( da_W^{[L]} \odot df^{[L]} \left( z_W^{[L]} \right) \bullet \frac{1}{\tau^{[L]}} \right) \left( \tau^{[L-1]} \bullet a_W^{[L-1]} \right)^T \\ &= \tau^{[L-1]} \bullet \left( da_W^{[L]} \odot df^{[L]} \left( z_W^{[L]} \right) a_W^{[L-1]} \right) \bullet \frac{1}{\tau^{[L]}} \\ &= \tau^{[L-1]} \bullet dW^{[L]} \bullet \frac{1}{\tau^{[L]}}. \end{aligned}$$

We then observe that

$$\begin{aligned} da_V^{[L-1]} &= (V^{[L]})^T da_V^{[L]} \\ &= \left( \tau^{[L]} \bullet (W^{[L]})^T \bullet \frac{1}{\tau^{[L-1]}} \right) \left( da_W^{[L]} \bullet \frac{1}{\tau^{[L]}} \right) \\ &= (W^{[L]})^T da_W^{[L]} \bullet \frac{1}{\tau^{[L-1]}} \\ &= da_W^{[L-1]} \bullet \frac{1}{\tau^{[L-1]}}. \end{aligned}$$

For the inductive step, we assume the result to be true for layers  $L+1, \dots, \ell+1$ . We will prove the result holds for layer  $\ell$ .

Indeed,

$$\begin{aligned}
dV^{[\ell]} &= \left( da_V^{[\ell]} \odot dg^{[\ell]}(z_V^{[\ell]}) \right) a_V^{[\ell-1]^T} \\
&= \left( da_W^{[\ell]} \bullet \frac{1}{\tau^{[\ell]}} \right) \odot df^{[\ell]} \left( z_W^{[\ell]} \bullet \tau^{[\ell]} \bullet \frac{1}{\tau^{[\ell]}} \right) a_V^{[\ell-1]^T} \\
&= \left( da_W^{[\ell]} \odot df^{[\ell]}(z_W^{[\ell]}) \bullet \frac{1}{\tau^{[\ell]}} \right) \left( a_W^{[\ell-1]} \bullet \tau^{[\ell-1]} \right)^T \\
&= \left( da_W^{[\ell]} \odot df^{[\ell]}(z_W^{[\ell]}) \right) \left( \tau^{[\ell-1]} \bullet a_W^{[\ell-1]^T} \right) \bullet \frac{1}{\tau^{[\ell]}} \\
&= \tau^{[\ell-1]} \bullet \left( da_W^{[\ell]} \odot df^{[\ell]}(z_W^{[\ell]}) \right) a_W^{[\ell-1]^T} \bullet \frac{1}{\tau^{[\ell]}} \\
&= \tau^{[\ell-1]} \bullet dW^{[\ell]} \bullet \frac{1}{\tau^{[\ell]}}.
\end{aligned}$$

It can be appreciated that back-propagation on  $(V, g)$  computes a re-scaling of the gradient of  $(W, f)$  by the CoB, just as claimed in the statement of the theorem. ■